Energy Level Realignment in Weakly Interacting Donor–Acceptor Binary Molecular Networks

Jian-Qiang Zhong,[†,∥] Xinming Qin,[‡,∥] Jia-Lin Zhang,[†] Satoshi Kera,[§] Nobuo Ueno,[§] Andrew Thye Shen Wee,[†] Jinlong Yang,[‡,*] and Wei Chen[†,⊥,#,*]

[†]Department of Physics, National University of Singapore, 2 Science Drive 3, 117542, Singapore, [‡]Division of Theoretical and Computational Sciences, Hefei National Laboratory for Physical Sciences at the Microscale, University of Science & Technology of China, Hefei, Anhui, 230026, People's Republic of China, [§]Graduate School of Advanced Integration Science, Chiba University, Chiba, 263-8522, Japan, [⊥]Department of Chemistry, National University of Singapore, 3 Science Drive 3, 117543, Singapore, and [#]National University of Singapore (Suzhou) Research Institute, Suzhou, 215123, People's Republic of China. [∥]J.-Q. Zhong and X. Qin contributed equally to this paper.

ABSTRACT Understanding the effect of intermolecular and molecule–substrate interactions on molecular electronic states is key to revealing the energy level alignment mechanism at organic–organic heterojunctions or organic–inorganic interfaces. In this paper, we investigate the energy level alignment mechanism in weakly interacting donor–acceptor binary molecular superstructures, comprising copper hexadecafluorophthalocyanine (F_{16}CuPc) intermixed with copper phthalocyanine (CuPc), or manganese phthalocynine (MnPc) on graphite. The molecular electronic structures have been systematically studied by *in situ* ultraviolet photoelectron spectroscopy (UPS) and low-temperature scanning tunneling microscopy/spectroscopy (LT-STM/STS) experiments and corroborated by density functional theory (DFT) calculations. As demonstrated by the UPS and LT-STM/STS measurements, the observed unusual energy level realignment (*i.e.*, a large downward shift in donor HOMO level and a corresponding small upward shift in acceptor HOMO level) in the CuPc–F_{16}CuPc binary superstructures originates from the balance between intermolecular and molecule–substrate interactions. The enhanced intermolecular interactions through the hydrogen bonding between neighboring CuPc and F_{16}CuPc can stabilize the binary superstructures and modify the local molecular electronic states. The obvious molecular energy level shift was explained by gap-state-mediated interfacial charge transfer.

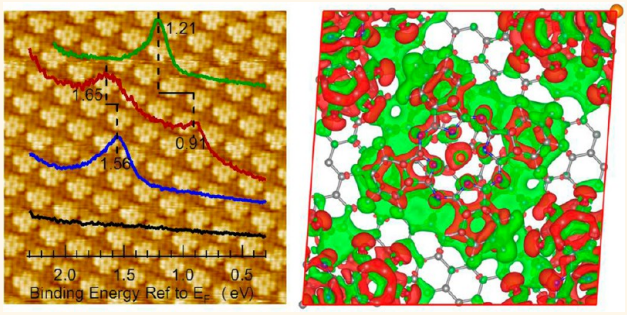

KEYWORDS: binary molecular superstructures · self-assembly · energy level alignment · gap states · weak intermolecular interactions · ultraviolet photoelectron spectroscopy · scanning tunneling microscopy

Impressive progress has been made on the controlled assembly of various functional molecules into well-ordered superstructures over the past decades,[1] for their potential applications in molecular electronics.[2] Fabrication of these self-assembled molecular superstructures is mainly controlled by the interplay of multiple interactions between the substrate and the adsorbed molecules, including the strong covalent bonding[3,4] and selective and directional noncovalent interactions, such as weak hydrogen bonding[5,6] and van der Waals interactions.[7,8] In particular, it has already been widely demonstrated that the weak hydrogen bonding and van der Waals interactions play essential roles in the formation of various self-assembled two-dimensional (2D) binary superstructures.[9–13] Most research efforts are mainly focused on the molecular self-assembly process and the fabrication of the novel molecular nanostructures; however, the understanding of the weak intermolecular interactions on the local molecular electronic states is very limited.

Recently, studies have been devoted to the understanding of the importance of weak noncovalent bond interactions on the performance of molecular electronics,[14,15] as well as the effect of weak intermolecular and molecule–substrate interactions on the energy level alignment in different donor–acceptor assemblies.[16–19] For example, Oteyza *et al.* observed the hybridization and charge transfer behavior in binary assemblies of copper

* Address correspondence to phycw@nus.edu.sg (W. Chen); jlyang@ustc.edu.cn (J. L. Yang).

Received for review November 24, 2013 and accepted January 13, 2014.

Published online 10.1021/nn406050e

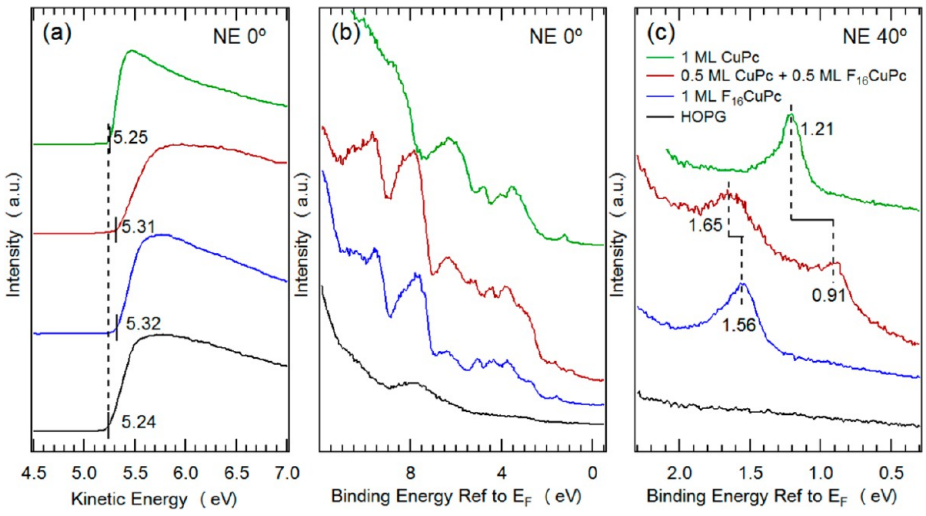

Figure 1. UPS spectra for a CuPc and F_{16}CuPc monolayer and their 1:1 mixture on a HOPG substrate. (a) UPS spectra at the low-kinetic-energy part with a −5 V sample bias (*i.e.*, secondary electron cutoff), (b) valence band spectra at the low-binding-energy part, and (c) corresponding close-up spectra in the HOMO band region. The photoelectron takeoff angles relative to the analyzer are indicated in the figures (NE 0° for photoelectron emission angle of 0°, *i.e.*, normal emission, while NE 40° for photoelectron emission angle of 40°). All binding energies are relative to the substrate E_F.

hexadecafluorophthalocyanine (F_{16}CuPc) and diindenoperylene (DIP) mediated through molecule−metal interactions.[13,18] To evaluate the molecular energy levels in the donor−acceptor complexes, Cabellos *et al.* have developed an effective approach to assess the charge transfer behavior in 2D donor−acceptor binary superstructures from X-ray photoelectron spectroscopy (XPS) core level shifts.[19,20] However, many reported self-assembled superstructures were prepared on metal surfaces, which involve relatively strong coupling between the metal d-electrons and the molecular π-orbitals.[18] The existence of interface hybrid electronic states as well as the non-negligible electron "push-back" effect on the metal surface can significantly affect the acquisition of intrinsic valence band information from the ultraviolet photoelectron spectroscopy (UPS) spectra,[21,22] thereby complicating the understanding of the intrinsic energy level alignment at organic donor/acceptor heterojunction interfaces in self-assembled 2D binary superstructures. By using layered inert graphite as substrate, the formation of hybrid interface electronic states can be largely suppressed, thereby serving as an ideal model system to probe the intrinsic molecular electronic states.[23]

In this paper, we investigate the mechanism of weak intermolecular interaction induced energy level realignment in self-assembled binary superstructures at the molecular scale, using model systems of F_{16}CuPc intermixed with copper phthalocyanine (CuPc), or manganese phthalocynine (MnPc) on highly oriented pyrolytic graphite (HOPG). The molecular electronic structures were systematically studied through the combination of *in situ* UPS, low-temperature scanning tunneling microscopy/spectroscopy (LT-STM/STS) experiments, and density functional theory (DFT) calculations. We find that the formation of weak intermolecular hydrogen bonds between neighboring donor and acceptor molecules can significantly perturb the interplay between intermolecular and molecule−substrate interfacial interactions and induce an unusual energy level realignment in self-assembled binary molecular superstructures, mediated through interfacial charge transfer *via* gap states.

RESULTS AND DISCUSSION

To understand the effect of weak hydrogen bonding on the molecular electronic states in self-assembled donor/acceptor binary networks, we first investigated the interfacial electronic structures of CuPc−F_{16}CuPc/HOPG using *in situ* UPS experiments. Mixed binary superstructures with a CuPc:F_{16}CuPc ratio of 1:1 were carefully prepared.[10] Chessboard-like patterns can be formed, steered by the intermolecular C−F···H−C hydrogen bonding between the neighboring CuPc and F_{16}CuPc, as reported in our previous STM measurements and molecular dynamic simulations [Figure S1(c) and S1(f)].[10] Interestingly, the assemblies revealed significant changes in molecular energy levels as shown in Figure 1. The vacuum levels (VL) of all well-ordered monolayers (*i.e.*, CuPc/HOPG, F_{16}CuPc/HOPG, binary/HOPG) were measured by the linear extrapolation of the low-kinetic-energy onset (secondary electron cutoff) of UPS spectra (Figure 1a). Small VL shifts were observed at these interfaces. In particular, at the interface between monolayer F_{16}CuPc and HOPG, a small upward VL shift of 0.08 eV was observed, suggesting the existence of a weak interfacial charge transfer.[24,25] The degree of the interfacial charge transfer can be roughly estimated from the Helmholtz equation[26,27] to be ~0.156 electron per molecule from HOPG to F_{16}CuPc (details can be found in the Supporting Information).

The valence band evolution is shown in Figure 1b and c. For a single-component monolayer on a HOPG substrate, their highest occupied molecular orbital (HOMO) peaks are centered at the binding energies of 1.56 eV (F_{16}CuPc/HOPG) and 1.21 eV (CuPc/HOPG), respectively. Different HOMO positions as well as the VL evolutions are mainly attributed to their different ionization potentials and can be well understood using the reported gap states model.[28−31] However, the valence band features for the weakly interacting CuPc−F_{16}CuPc binary assemblies are not a simple superposition of individual components. As shown by the brown spectrum in Figure 1c, the F_{16}CuPc-related HOMO peak slightly shifts to higher binding energy by ~0.09 eV, while the CuPc-related HOMO peak largely shifts to lower binding energy by ~0.30 eV and toward the Fermi level (E_F). This suggests that the molecular electronic states in the binary superstructures can be significantly perturbed by the local lateral intermolecular interactions between CuPc and F_{16}CuPc, even though such interaction is considered to be very weak.[1,16−20,32]

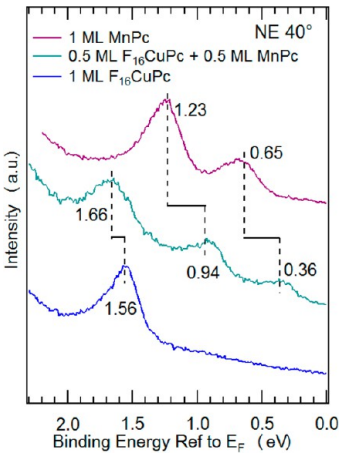

Figure 2. UPS spectra in the HOMO band region for a MnPc and F_{16}CuPc monolayer and their 1:1 mixture on a HOPG substrate, respectively. Both the Mn 3d derived HOMO state (0.65 eV) and ligand π-orbital-induced HOMO state (1.23 eV) shift to the low-binding-energy region by 0.29 eV in the binary network.

Similar energy level alignments can also be observed in another 2D binary donor/acceptor superstructure of manganese phthalocyanine (MnPc) intermixed with F_{16}CuPc (Figure 2). As shown in Figure 2, MnPc is chosen as the donor molecule due to its Mn 3d derived HOMO state,[33] appearing at 0.65 eV below the

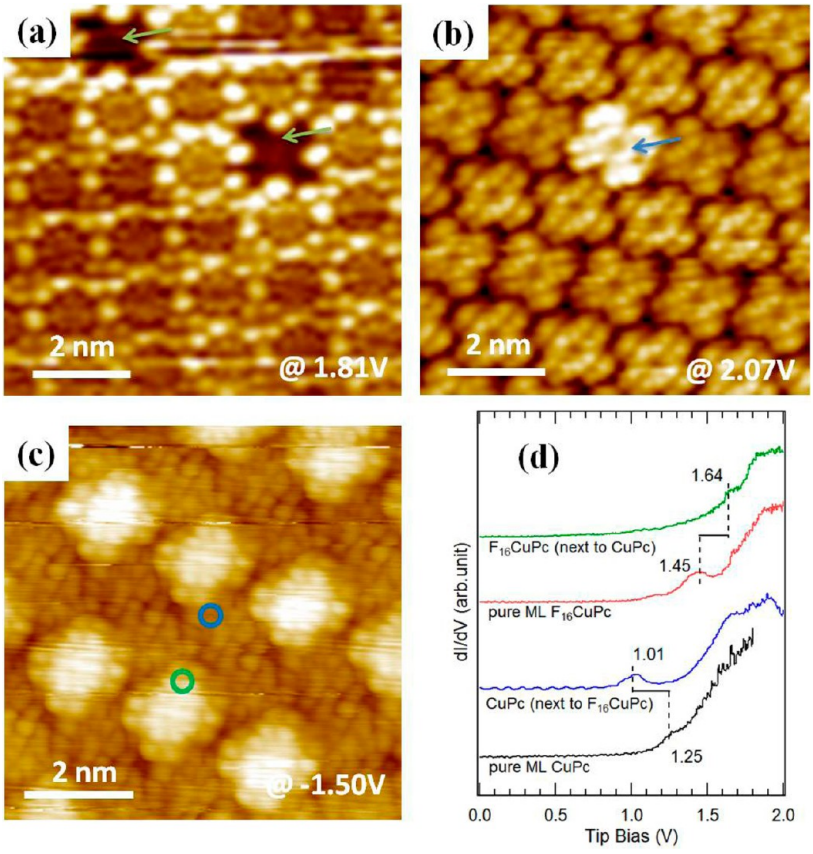

Figure 3. STM images of (a) two F_{16}CuPc molecules embedded in the CuPc monolayer on HOPG (V_{tip} = 1.81 V, 10 × 10 nm^2; the dark features refer to the F_{16}CuPc molecules) and (b) one CuPc molecule embedded in the F_{16}CuPc monolayer on HOPG (V_{tip} = 2.07 V, 10 × 10 nm^2; the bright feature refers to the CuPc molecule). (c) Supramolecular packing structure of CuPc−F_{16}CuPc binary network with intermixing ratio of 2:1. (V_{tip} = −1.50 V, 8 × 8 nm^2; here, the dark and bright features refer to the CuPc and F_{16}CuPc molecules, respectively). (d) STS spectra taken at the lobe of F_{16}CuPc molecules and CuPc molecules for both pure and mixed molecular layers.

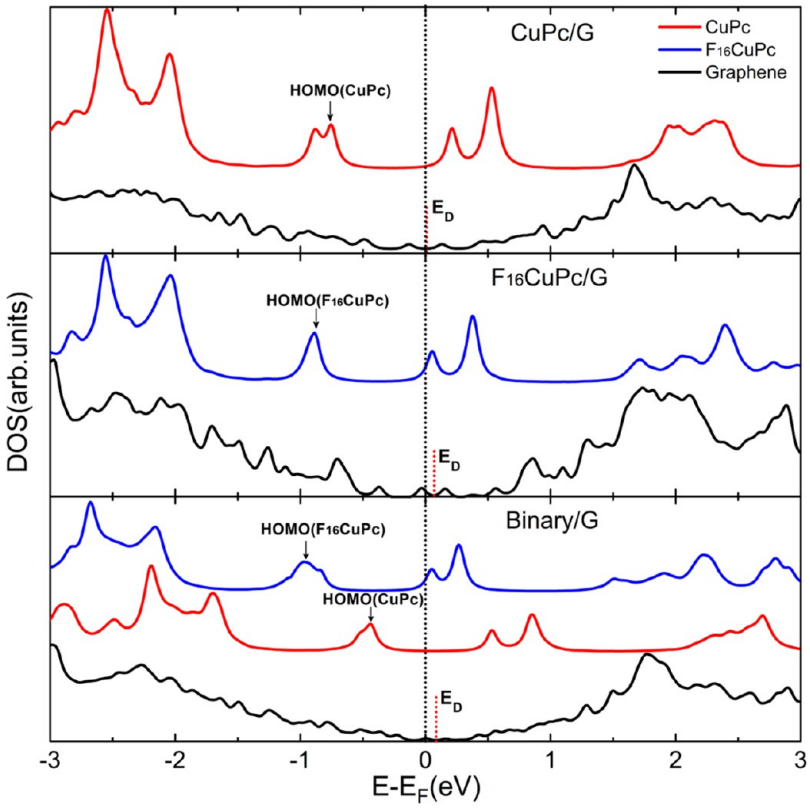

Figure 4. Projected DOS for the monolayer of CuPc, F_{16}CuPc, and their 1:1 mixture absorbed on a graphene substrate. The Fermi level is set to zero, and the red dotted lines mark the Dirac point of graphene.

E_F. The next feature centered at 1.23 eV is assigned to the ligand π-orbital. The evolution of the HOMO levels in the binary assemblies shows a similar trend to that of CuPc−F_{16}CuPc, *i.e.*, the MnPc-related HOMOs largely shift toward E_F by 0.29 eV; in contrast, the F_{16}CuPc-related HOMO again slightly shifts to higher binding energy by 0.10 eV.

To further examine the significant HOMO shift in these well-ordered 2D binary superstructures, we studied the local electronic states of CuPc−F_{16}CuPc assemblies on HOPG using *in situ* LT-STM/STS measurements. As previously reported, both CuPc and F_{16}CuPc molecules lie flat on HOPG with their molecular planes parallel to the substrate due to the interfacial $\pi-\pi$ interaction.[10,34] The packing structures can be well controlled by tuning the relative ratio of the molecules.[9,20] Besides visualizing molecular aggregation and ordering, STM images also provide information on the local surface electronic states of various adsorbates from bias-dependent measurements.[10] In Figure 3a and b, the molecularly resolved STM images reveal the changes of local electronic states of the CuPc−F_{16}CuPc assemblies. Figure 3a shows the STM image of two F_{16}CuPc molecules embedded into the CuPc monolayer on HOPG. Here, the two darker features are assigned to F_{16}CuPc molecules for its deep HOMO state (Figure 1c). Interestingly, the CuPc molecules neighboring the F_{16}CuPc appear much brighter than that of other CuPc molecules, suggesting that their electronic structures have been significantly perturbed by the neighboring F_{16}CuPc. By a similar argument, in the STM image shown in Figure 3b, one CuPc molecule (the brighter one) is randomly embedded into the F_{16}CuPc monolayer. However, in this case, the local electronic states of the surrounding F_{16}CuPc are not obviously affected by the embedded CuPc. The STM results demonstrate that the intrinsic electronic states of CuPc can be significantly modulated in the assemblies, in good agreement with the HOMO level shift as revealed by the UPS measurements shown in Figure 1c; that is, the degree of energy shift for the CuPc HOMO (0.30 eV to lower binding energy region) was much larger than that of F_{16}CuPc (0.09 eV to higher binding energy region).

STS measurements were also taken at all these interfaces to measure local electronic density of states (DOS). Figure 3c displays the molecularly resolved STM image of the well-organized CuPc−F_{16}CuPc binary network with an intermixing ratio of 2:1. The brighter features here correspond to the F_{16}CuPc molecules at negative tip bias. STS spectra were collected at the lobe of each organic molecule as highlighted by the blue and green circles in Figure 3c. The obtained spectra in Figure 3d were averaged over 30 STS spectra taken at similar positions in this binary superstructure. For comparison, the electronic structures of a

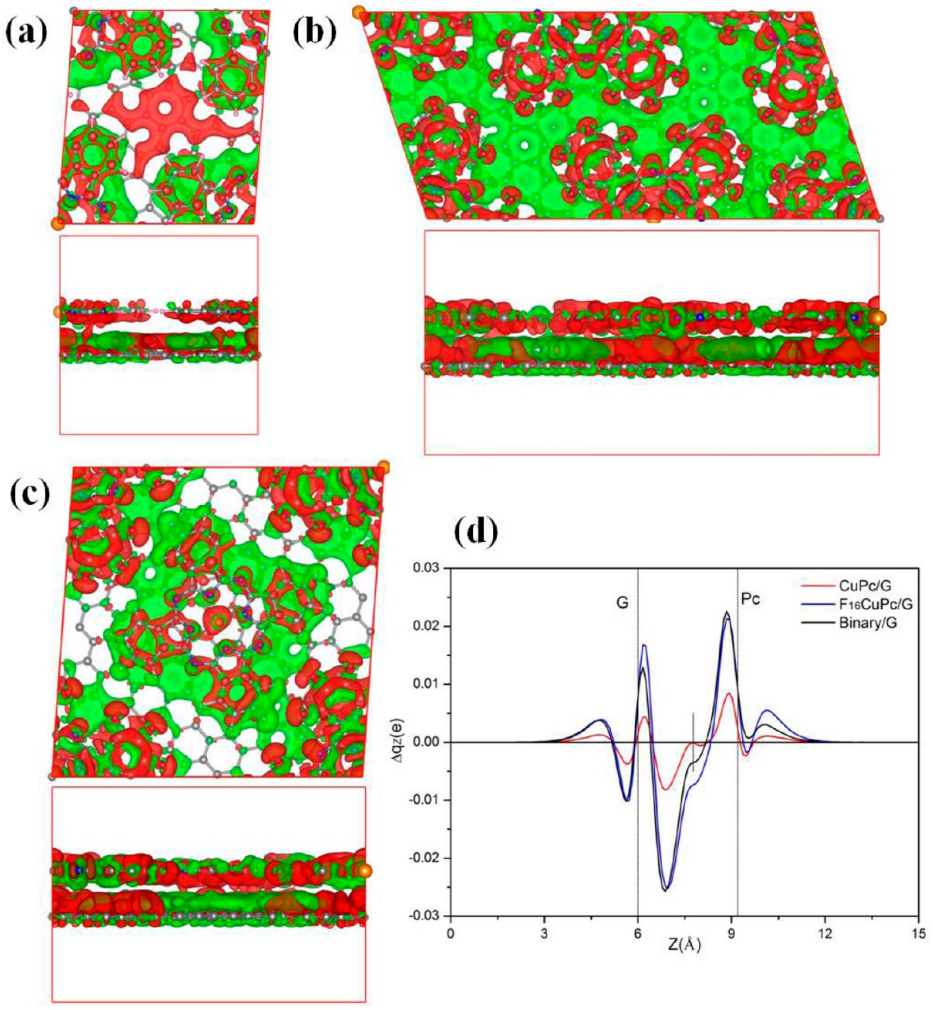

Figure 5. Top view and side view of the charge density difference for (a) CuPc/graphene[(1,5) × (4,3)], (b) F_{16}CuPc/graphene[(7,8) × (2,5)], and (c) binary/graphene[(3,7) × (7,3)] at contour levels of 0.002 e/Å. The red and green clouds correspond to regions with electron accumulation and depletion, respectively. (d) One-dimensional charge density difference along the surface normal direction of graphene; vertical lines mark the position of graphene and molecule planes.

single-component monolayer (*i.e.*, CuPc/HOPG, black spectrum; F_{16}CuPc/HOPG, red spectrum) are also shown in Figure 3d. Clearly, as compared with the single-component monolayer on HOPG, the CuPc-related HOMO peak shifts to lower binding energy by 0.24 eV and the F_{16}CuPc-related HOMO peak shifts to higher binding energy by 0.19 eV in this binary system. The degree of HOMO state shift differs slightly from the UPS results with a packing structure of 1:1 intermixing ratio, possibly originating from different supramolecular arrangements with different weak intermolecular bonding environments for the localized probing technique.

The UPS and LT-STM/STS results indicate that the local electronic states as well as the energy level alignment in these 2D binary assemblies can be modified by weak intermolecular interactions. We further explored the underlying mechanisms using first-principles calculations for the CuPc−F_{16}CuPc binary system adsorbed on graphene. During structural optimization (detailed packing structures can be found in Figure S1), the structures of all adsorbed molecules deviated from their ideal planar structures. For pure CuPc/graphene, the adsorption height for CuPc was 3.26 Å, which was the distance between the lowest Cu atom and graphene (the Cu atom was 0.04 Å lower than all other atoms). Different results were found for F_{16}CuPc/graphene, where the F atoms were 0.04 Å lower than the central Cu atom, and the adsorption height was 3.17 Å. For the binary monolayer, the Cu atoms in both CuPc and F_{16}CuPc molecules were at the same height of 3.22 Å above the graphene. The molecule adsorption energy was defined as[34]

$$E_a = (E_{total} - E_{graphene} - n \times E_{Pc})/n$$

where E_{total}, $E_{graphene}$, and E_{Pc} refer to the total energy of the adsorption system, the energy of the isolated graphene substrate, and the energy of gas phase phthalocyanine molecules, respectively, and n is the number of phthalocyanine molecules in the unit cell

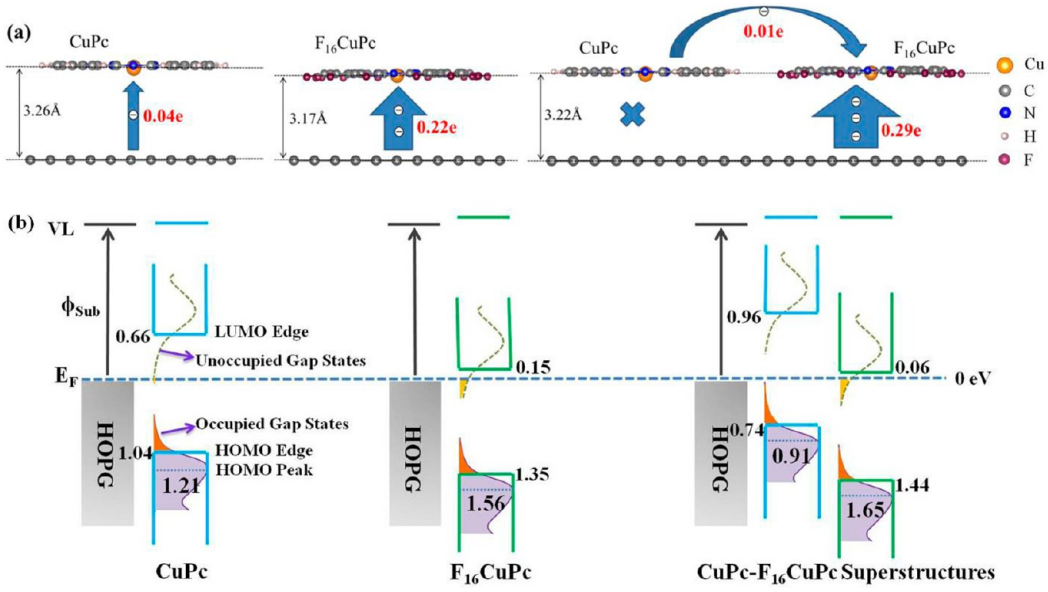

Figure 6. Schematic illustrations of gap-states-mediated weak interface charge transfer behaviors in explaining the significant energy level shift in weakly interacting binary molecular systems. The unoccupied and occupied gap states are indicated by the purple arrows in the figure, which are extended from the LUMO and HOMO edge, respectively, and decayed exponentially into the band gap.

(UC). Long-range dispersion corrections were included in the calculations of the total energies. The calculated adsorption energies for the CuPc, F_{16}CuPc, and their binary CuPc−F_{16}CuPc monolayers on graphene are E_a(CuPc) = −2.54 eV/UC, E_a(F_{16}CuPc) = −3.06 eV/UC, and E_a(CuP−F_{16}CuPc) = −2.90 eV/UC, corresponding to 44.6, 53.7, and 50.9 meV/atom, respectively. As previously reported, a dispersion force dominated interfacial interaction can lead to the interaction energy range of 35−60 meV/atom for the phthalocyanine−graphene system.[34,35] Large adsorption heights (~3.22 Å) and small adsorption energies (~50.9 meV/atom) reveal a weak interaction at the binary/graphene interface.

The molecular interface electronic structures of all absorption systems were calculated based on the aforementioned optimized structures (Figure S1). The projected DOS of the adsorbed molecules and graphene substrates are presented in Figure 4. The E_F in all adsorption systems was located below the Dirac point of graphene and shifted toward the lowest unoccupied molecular orbital (LUMO) of the adsorption molecules: E_F in CuPc/graphene was close to the LUMO of CuPc, while E_F in F_{16}CuPc/graphene almost crossed the LUMO of F_{16}CuPc. These results indicate small electron transfer from substrate to molecules. The amount of electron transfer in F_{16}CuPc/graphene was larger than that of CuPc/graphene. From the projected DOS, the CuPc-related HOMO shifted 0.28 eV toward E_F from the CuPc/graphene system to the binary/graphene system, but the F_{16}CuPc-related HOMO was shifted 0.05 eV away from E_F, in good agreement with the experimental results.

In order to gain more insight into the weak electronic interactions between the absorbed molecules and graphene, the corresponding charge density differences (CDD) were also calculated (Figure 5; their corresponding unit cell structure can be seen in Figure S1). The CDD was defined as[34]

$$\rho = \rho_{total} - \rho_{Pc} - \rho_{graphene}$$

where ρ_{total}, ρ_{Pc}, and $\rho_{graphene}$ refer to the charge density of the combined system, isolated phthalocyanine molecule, and graphene with geometries optimized for the adsorption system, respectively. The amount of electron transfer from graphene to phthalocyanine molecules was obtained by integrating the CDD along the surface normal direction *z*, *i.e.*, 0.04*e* for CuPc/graphene and 0.22*e* for F_{16}CuPc/graphene, respectively. The results were consistent with the estimations from the Helmholtz equation and the PDOS as displayed in Figure 4 (a much closer E_F relative to the Dirac point of graphene). One-dimensional CDD shown in Figure 5d also exhibits a relative larger dipole at the F_{16}CuPc/graphene interface. Interestingly, for the binary/graphene system, the Bader charge analysis showed 0.01*e* and 0.28*e* electron lost in the CuPc molecule and graphene substrate, respectively, while 0.29*e* electron gained in each F_{16}CuPc molecule. Clearly, the electron transfer flow between CuPc and HOPG was changed from receiving 0.04*e* (CuPc/graphene) to losing 0.01*e* (binary/graphene), possibly originating from the perturbation by neighboring F_{16}CuPc molecules and the formation of weak intermolecular hydrogen bonding. This change would

result in a significant HOMO level shift (toward E_F) as shown in the UPS spectra and the PDOS.

The large HOMO level shift (~0.30 eV) can be well explained using the gap states model (Figure 6; the LUMO was derived from the reported HOMO−LUMO gap[34,36−38]). As previously reported, the density of gap states decays exponentially as a function of energy from the HOMO or LUMO edge, which extends several hundred meV into the band gap.[39] Upon the formation of the binary system, the charge transfer direction between CuPc and graphene was reversed, and hence the E_F shifted from the bottom of the unoccupied gap states (CuPc/graphene) to the top of the occupied gap states (binary/graphene) in CuPc, thereby inducing a large HOMO shift as observed in Figure 1c and the schematic diagram in Figure 6. F_{16}CuPc received more electrons in the binary system. However, because of the large density of gap states near the LUMO edge in F_{16}CuPc, the integration of the small range of unoccupied gap states below LUMO was sufficient to accommodate the electrons transferred from HOPG to reach thermodynamic equilibrium (as shown by the schematic in Figure 6), thereby resulting in a small molecular orbital shift, *i.e.*, small HOMO shift observed in Figure 1c.

CONCLUSION

We have investigated the mechanism of weak intermolecular interaction induced HOMO level shift in self-assembled binary superstructures based on *in situ* UPS, LT-STM/STS measurements, and first-principles calculations. Our studies elucidated the effects of balanced intermolecular and molecule−substrate interactions on the interface charge transfer behaviors and local electronic states. Although the hydrogen-bonding interactions were demonstrated to be weak by both experimental measurements and DFT calculations, the molecular energy levels can be significantly affected through the gap-states-mediated interfacial charge transfer. Our results can help reveal the importance of weak intermolecular interactions on the molecular electronic states and shed light on exploring and designing new molecular nanostructures with desired functionalities.

METHODS

In situ photoelectron spectroscopy (PES) experiments were carried out in a custom-designed ultrahigh vacuum (UHV) system with a base pressure better than 2×10^{-10} mbar.[40,41] He Iα ($h\nu$ = 21.2 eV) and Mg Ka ($h\nu$ =1253.6 eV) were used as the excitation sources for UPS and XPS, respectively. Vacuum level shifts were determined from the secondary electron cutoff at the low kinetic energy part of the UPS spectra with a −5 V sample bias. All UPS and XPS measurements were performed at room temperature (RT), and the binding energies of all PES spectra were calibrated and referenced to the Fermi level of a sputter-cleaned Ag(110) substrate. The total instrumental energy resolution was estimated to be about 100 meV for UPS (the energy difference measured between 12% and 88% of the intensity from the Fermi edge of a clean Ag(110) substrate) and 850 meV for XPS (the full width at half-maximum of the Ag 3d peak). The LT-STM/STS experiments were performed in a multichamber UHV system housing an Omicron LT-STM. STM imaging was carried out at 77 K in constant current mode with a chemically etched tungsten tip.

Fresh cleaved HOPG (Mateck/ZYA-grade) substrate was thoroughly degassed in the UHV chamber at around 800 K overnight before molecule deposition. Vacuum-sublimated purified organic molecules were thermally evaporated onto the HOPG substrate at RT from separate Knudsen cells in the growth chamber (base pressure $<1 \times 10^{-9}$ mbar). The deposition rates were monitored by a quartz crystal microbalance during evaporation and were further calibrated by counting the adsorbed molecule coverage in the large-scale STM images at a coverage below 1 monolayer.

Theoretical calculations were performed using VASP code[42−44] with the projector-augmented wave (PAW) potentials.[45,46] Generalized gradient corrections were applied to the exchange−correlation functional within the implementation of Perdew, Burke, and Ernzerhof (PBE).[47] Long-range dispersion corrections were considered within the semiempirical DFT-D2 method.[48] After the full convergence test, the kinetic energy cutoff of the plane wave basis was chosen to be 500 eV. Brillouin zones of the superstructures of monolayer CuPc, F_{16}CuPc, and CuPc−F_{16}CuPc on graphene were sampled in the k-space within the Monkhorst−Pack scheme[49] by ($4 \times 4 \times 1$), ($2 \times 4 \times 1$), and ($4 \times 4 \times 1$) mesh points, respectively. For geometry optimization, all atomic positions were fully relaxed using the conjugate gradient method when Hellmann−Feynman forces were smaller than 0.02 eV/Å.

Conflict of Interest: The authors declare no competing financial interest.

Acknowledgment. The authors acknowledge the financial support from Singapore MOE Grant R143-000-559-112, NUS-YIA Grant R143-000-452-101, Global COE Program (G-03, MEXT, Japan), KAKENHI of Japan (23360005 and 24245034), the National Key Basic Research Program of China (Grant No. 2011CB921404), and Chinese Academy of Sciences (CAS) (Grant No. XDB01020300).

Supporting Information Available: Figure S1, STM images and calculated supramolecular packing structures for CuPc, F_{16}CuPc, and their binary network; Figure S2, atomic structures and the energy levels of the isolated CuPc and F_{16}CuPc molecules; Figure S3, UPS spectra for MnPc−F_{16}CuPc system; Figure S4, XPS spectra for MnPc−F_{16}CuPc system; Figure S5, UPS spectra in the HOMO band region for CuPc:F_{16}CuPc intermixing ratios of 1:2, 1:1, and 2:1. These materials are available free of charge *via* the Internet at http://pubs.acs.org.

REFERENCES AND NOTES

1. Zhang, J. L.; Niu, T. C.; Wee, A. T. S.; Chen, W. Self-Assembly of Binary Molecular Nanostructure Arrays on Graphite. *Phys. Chem. Chem. Phys.* **2013**, *15*, 12414–12427.
2. Ratner, M. A Brief History of Molecular Electronics. *Nat. Nanotechnol.* **2013**, *8*, 378–381.
3. Grill, L.; Dyer, M.; Lafferentz, L.; Persson, M.; Peters, M. V.; Hecht, S. Nano-architectures by Covalent Assembly of Molecular Building Blocks. *Nat. Nanotechnol.* **2007**, *2*, 687–691.
4. Zwaneveld, N. A. A.; Pawlak, R. M.; Abel, M.; Catalin, D.; Gigmes, D.; Bertin, D.; Porte, L. Organized Formation of 2D Extended Covalent Organic Frameworks at Surfaces. *J. Am. Chem. Soc.* **2008**, *130*, 6678–6679.
5. Pawin, G.; Wong, K. L.; Kwon, K.-Y.; Bartels, L. A Homomolecular Porous Network at a Cu(111). *Surf. Sci.* **2006**, *313*, 961–962.

6. Schnadt, J.; Rauls, E.; Xu, W.; Vang, R. T.; Knudsen, J.; Lægsgaard, E.; Li, Z.; Hammer, B.; Besenbacher, F. Extended One-Dimensional Supramolecular Assembly on a Stepped Surface. *Phys. Rev. Lett.* **2008**, *100*, 046103.
7. Mao, J.; Zhang, H.; Jiang, Y.; Pan, Y.; Gao, M.; Xiao, W.; Gao, H. J. Tunability of Supramolecular Kagome Lattices of Magnetic Phthalocyanines Using Graphene-Based Moiré Patterns as Templates. *J. Am. Chem. Soc.* **2009**, *131*, 14136–14137.
8. Tahara, K.; Lei, S.; Adisoejoso, J.; De Feyter, S.; Tobe, Y. Supramolecular Surface-Confined Architectures Created by Self-Assembly of Triangular Phenylene-Ethynylene Macrocycles *via* Van Der Waals Interaction. *Chem. Commun.* **2010**, *46*, 8507–8525.
9. Huang, Y. L.; Chen, W.; Li, H.; Ma, J.; Pflaum, J.; Wee, A. T. S. Tunable Two-Dimensional Binary Molecular Networks. *Small* **2010**, *6*, 70–75.
10. Huang, Y. L.; Li, H.; Ma, J.; Huang, H.; Chen, W.; Wee, A. T. S. Scanning Tunneling Microscopy Investigation of Self-Assembled CuPc/F16CuPc Binary Superstructures on Graphite. *Langmuir* **2009**, *26*, 3329–3334.
11. Huang, Y. L.; Chen, W.; Wee, A. T. S. Molecular Trapping on Two-Dimensional Binary Supramolecular Networks. *J. Am. Chem. Soc.* **2010**, *133*, 820–825.
12. Niu, T. C.; Huang, Y. L.; Sun, J. T.; Kera, S.; Ueno, N.; Wee, A. T. S.; Chen, W. Tunable Two-Dimensional Molecular Dipole Dot Arrays on Graphite. *Appl. Phys. Lett.* **2011**, *99*, 143114.
13. de Oteyza, D. G.; Silanes, I.; Ruiz-Osés, M.; Barrena, E.; Doyle, B. P.; Arnau, A.; Dosch, H.; Wakayama, Y.; Ortega, J. E. Balancing Intermolecular and Molecule−Substrate Interactions in Supramolecular Assemblies. *Adv. Funct. Mater.* **2009**, *19*, 259–264.
14. Nerngchamnong, N.; Yuan, L.; Qi, D.-C.; Li, J.; Thompson, D.; Nijhuis, C. A. The Role of Van Der Waals Forces in the Performance of Molecular Diodes. *Nat. Nanotechnol.* **2013**, *8*, 113–118.
15. Isono, T.; Kamo, H.; Ueda, A.; Takahashi, K.; Nakao, A.; Kumai, R.; Nakao, H.; Kobayashi, K.; Murakami, Y.; Mori, H. Hydrogen Bond-promoted Metallic State in a Purely Organic Single-Component Conductor under Pressure. *Nat. Commun.* **2013**, *4*, 1344.
16. El-Sayed, A.; Mowbray, D. J.; García-Lastra, J. M.; Rogero, C.; Goiri, E.; Borghetti, P.; Turak, A.; Doyle, B. P.; Dell'Angela, M.; Floreano, L.; *et al.* Supramolecular Environment-Dependent Electronic Properties of Metal−Organic Interfaces. *J. Phys. Chem. C* **2012**, *116*, 4780–4785.
17. Ruiz-Osés, M.; de Oteyza, D. G.; Fernández-Torrente, I.; Gonzalez-Lakunza, N.; Schmidt-Weber, P. M.; Kampen, T.; Horn, K.; Gourdon, A.; Arnau, A.; Ortega, J. E. Non-Covalent Interactions in Supramolecular Assemblies Investigated with Electron Spectroscopies. *ChemPhysChem* **2009**, *10*, 896–900.
18. de Oteyza, D. G.; García-Lastra, J. M.; Corso, M.; Doyle, B. P.; Floreano, L.; Morgante, A.; Wakayama, Y.; Rubio, A.; Ortega, J. E. Customized Electronic Coupling in Self-Assembled Donor−Acceptor Nanostructures. *Adv. Funct. Mater.* **2009**, *19*, 3567–3573.
19. Cabellos, J. L.; Mowbray, D. J.; Goiri, E.; El-Sayed, A.; Floreano, L.; de Oteyza, D. G.; Rogero, C.; Ortega, J. E.; Rubio, A. Understanding Charge Transfer in Donor−Acceptor/Metal Systems: A Combined Theoretical and Experimental Study. *J. Phys. Chem. C* **2012**, *116*, 17991–18001.
20. El-Sayed, A.; Borghetti, P.; Goiri, E.; Rogero, C.; Floreano, L.; Lovat, G.; Mowbray, D. J.; Cabellos, J. L.; Wakayama, Y.; Rubio, A.; *et al.* Understanding Energy-Level Alignment in Donor−Acceptor/Metal Interfaces from Core-Level Shifts. *ACS Nano* **2013**, *7*, 6914–6920.
21. Amsalem, P.; Niederhausen, J.; Frisch, J.; Wilke, A.; Bröker, B.; Vollmer, A.; Rieger, R.; Müllen, K.; Rabe, J. R. P.; Koch, N. Metal-to-Acceptor Charge Transfer through a Molecular Spacer Layer. *J. Phys. Chem. C* **2011**, *115*, 17503–17507.
22. Niederhausen, J.; Amsalem, P.; Wilke, A.; Schlesinger, R.; Winkler, S.; Vollmer, A.; Rabe, J. P.; Koch, N. Doping of C60 Monolayers by Fermi-Level Pinning Induced Electron Transfer. *Phys. Rev. B* **2012**, *86*, 081411.
23. Ortmann, F.; Schmidt, W. G.; Bechstedt, F. Attracted by Long-Range Electron Correlation: Adenine on Graphite. *Phys. Rev. Lett.* **2005**, *95*, 186101.
24. Zhong, J. Q.; Mao, H. Y.; Wang, R.; Qi, D. C.; Cao, L.; Wang, Y. Z.; Chen, W. Effect of Gap States on the Orientation-Dependent Energy Level Alignment at the DIP/F16CuPc Donor−Acceptor Heterojunction Interfaces. *J. Phys. Chem. C* **2011**, *115*, 23922–23928.
25. Yamane, H.; Yabuuchi, Y.; Fukagawa, H.; Kera, S.; Okudaira, K. K.; Ueno, N. Does the Molecular Orientation Induce an Electric Dipole in Cu-Phthalocyanine Thin Films? *J Appl. Phys.* **2006**, *99*, 093705.
26. Fukagawa, H.; Kera, S.; Kataoka, T.; Hosoumi, S.; Watanabe, Y.; Kudo, K.; Ueno, N. The Role of the Ionization Potential in Vacuum-Level Alignment at Organic Semiconductor Interfaces. *Adv. Mater.* **2007**, *19*, 665–668.
27. Fukagawa, H.; Yamane, H.; Kera, S.; Okudaira, K. K.; Ueno, N. Experimental Estimation of the Electric Dipole Moment and Polarizability of Titanyl Phthalocyanine Using Ultraviolet Photoelectron Spectroscopy. *Phys. Rev. B* **2006**, *73*, 041302.
28. Zhong, S.; Zhong, J. Q.; Mao, H. Y.; Zhang, J. L.; Lin, J. D.; Chen, W. The Role of Gap States in the Energy Level Alignment at the Organic-Organic Heterojunction Interfaces. *Phys. Chem. Chem. Phys.* **2012**, *14*, 14127–14141.
29. Bussolotti, F.; Kera, S.; Kudo, K.; Kahn, A.; Ueno, N. Gap states in Pentacene Thin Film Induced by Inert Gas Exposure. *Phys. Rev. Lett.* **2013**, *110*, 267602.
30. Sueyoshi, T.; Fukagawa, H.; Ono, M.; Kera, S.; Ueno, N. Low-Density Band-Gap States in Pentacene Thin Films Probed with Ultrahigh-Sensitivity Ultraviolet Photoelectron Spectroscopy. *Appl. Phys. Lett.* **2009**, *95*, 183303.
31. Sueyoshi, T.; Kakuta, H.; Ono, M.; Sakamoto, K.; Kera, S.; Ueno, N. Band Gap States of Copper Phthalocyanine Thin Films Induced by Nitrogen Exposure. *Appl. Phys. Lett.* **2010**, *96*, 093303.
32. Otero, R.; Schöck, M.; Molina, L. M.; Lægsgaard, E.; Stensgaard, I.; Hammer, B.; Besenbacher, F. Guanine Quartet Networks Stabilized by Cooperative Hydrogen Bonds. *Angew. Chem., Int. Ed.* **2005**, *44*, 2270–2275.
33. Grobosch, M.; Mahns, B.; Loose, C.; Friedrich, R.; Schmidt, C.; Kortus, J.; Knupfer, M. Identification of the Electronic States of Manganese Phthalocyanine Close to the Fermi Level. *Chem. Phys. Lett.* **2011**, *505*, 122–125.
34. Ren, J.; Meng, S.; Wang, Y.-L.; Ma, X.-C.; Xue, Q.-K.; Kaxiras, E. Properties of Copper (Fluoro-)phthalocyanine Layers Deposited on Epitaxial Graphene. *J. Chem. Phys.* **2011**, *134*, 194706–10.
35. Grimme, S. Do Special Noncovalent $\pi-\pi$ Stacking Interactions Really Exist? *Angew Chem., Int. Ed.* **2008**, *47*, 3430–3434.
36. Lau, K. M.; Tang, J. X.; Sun, H. Y.; Lee, C. S.; Lee, S. T.; Yan, D. Interfacial Electronic Structure of Copper Phthalocyanine and Copper Hexadecafluorophthalocyanine Studied by Photoemission. *Appl. Phys. Lett.* **2006**, *88*, 173513–3.
37. Shen, C.; Kahn, A. Electronic Structure, Diffusion, and P-doping at the Au/F_{16}CuPc Interface. *J. Appl. Phys.* **2001**, *90*, 4549–4554.
38. Hill, I. G.; Kahn, A. Energy Level Alignment at Interfaces of Organic Semiconductor Heterostructures. *J. Appl. Phys.* **1998**, *84*, 5583–5586.
39. Lange, I.; Blakesley, J. C.; Frisch, J.; Vollmer, A.; Koch, N.; Neher, D. Band Bending in Conjugated Polymer Layers. *Phys. Rev. Lett.* **2011**, *106*, 216402.
40. Zhong, J. Q.; Huang, H.; Mao, H. Y.; Wang, R.; Zhong, S.; Chen, W. Molecular-Scale Investigation of C60/p-Sexiphenyl Organic Heterojunction Interface. *J. Chem. Phys.* **2011**, *134*, 154706–6.
41. Zhong, J. Q.; Mao, H. Y.; Wang, R.; Lin, J. D.; Zhao, Y. B.; Zhang, J. L.; Ma, D. G.; Chen, W. Ionization Potential Dependent Air Exposure Effect on the MoO_3/Organic Interface Energy Level Alignment. *Org. Electron.* **2012**, *13*, 2793–2800.
42. Kresse, G.; Hafner, J. Ab Initio Molecular Dynamics for Liquid Metals. *Phys. Rev. B* **1993**, *47*, 558–561.

43. Kresse, G.; Furthmüller, J. Efficient Iterative Schemes for ab Initio Total-energy Calculations Using A PPlane-Wave Basis Set. *Phys. Rev. B* **1996**, *54*, 11169–11186.
44. Kresse, G.; Furthmüller, J. Efficiency of ab-Initio Total Energy Calculations for Metals and Semiconductors Using a Plane-Wave Basis Set. *Comput. Mater. Sci.* **1996**, *6*, 15–50.
45. Blöchl, P. E. Projector Augmented-Wave Method. *Phys. Rev. B* **1994**, *50*, 17953–17979.
46. Kresse, G.; Joubert, D. From Ultrasoft Pseudopotentials to the Projector Augmented-Wave Method. *Phys. Rev. B* **1999**, *59*, 1758–1775.
47. Perdew, J. P.; Burke, K.; Ernzerhof, M. Generalized Gradient Approximation Made Simple. *Phys. Rev. Lett.* **1996**, *77*, 3865–3868.
48. Grimme, S. Semiempirical GGA-Type Density Functional Constructed with a Long-Range Dispersion Correction. *J. Comput. Chem.* **2006**, *27*, 1787–1799.
49. Monkhorst, H. J.; Pack, J. D. Special Points for Brillouin-Zone Integrations. *Phys. Rev. B* **1976**, *13*, 5188–5192.